Carbohydrate Polymers 90 (2012) 1771–1778

Contents lists available at SciVerse ScienceDirect

Carbohydrate Polymers

journal homepage: www.elsevier.com/locate/carbpol

Theoretical study on the mechanisms of cellulose dissolution and precipitation in the phosphoric acid–acetone process

Peng Kang, Wu Qin*, Zong-Ming Zheng, Chang-Qing Dong*, Yong-Ping Yang

National Engineering Laboratory for Biomass Power Generation Equipment, School of Renewable Energy Engineering, North China Electric Power University, Beijing 102206, PR China

ARTICLE INFO

Article history:
Received 5 June 2012
Received in revised form 19 July 2012
Accepted 26 July 2012
Available online 1 August 2012

Keywords:
Density functional theory
Dissolution
Lignocellulose
Molecular dynamic
Precipitation

ABSTRACT

Phosphoric acid–acetone fractionation was applied to pretreat lignocellulose for production of cellulosic ethanol. Cellulose solubility properties in H_2O, H_3PO_4 and CH_3COCH_3 were simulated. Atomic geometry and electronic properties were computed using density functional theory with local-density approximation. H_3PO_4 molecule is adsorbed between two cellulose segments, forming four hydrogen bonds with E_B of −1.61 eV. Density of state for cellulose in H_3PO_4–cellulose system delocalizes without obvious peak. E_{gap} of 4.46 eV is much smaller than that in other systems. Molecular dynamics simulation indicates that fragments of double glucose rings separate in the cellulose–H_3PO_4 interaction system. Icy CH_3COCH_3 addition leads to re-gathering of separated fragments. Reaction energy of cellulose in three solvents is around 3.5 eV, implying that cellulose is chemically stable. Moreover, theoretical results correspond to the experiments we have performed, showing that cellulose dissolves in H_3PO_4, flocculates after CH_3COCH_3 addition, and finally becomes more liable to be hydrolyzed into glucoses.

1. Introduction

Countries, governments, and individuals are increasingly concerning about energy security, resource depletion and environmental degradation. According to the recently released 2011 BP (British Petroleum Company) statistical review of world energy (British Petroleum Company, 2011), by the end of 2010, world's total proved reserves of oil is 188.8 billion tons. With current consumption trends, the reserves-to-production (R/P) ratio of world proved reserves of oil is only 46.2 years.

Biomass, the sustainable resource, is capable of delivering liquid fuels and chemical products on a large scale. US alone has the potential to produce more than 1.3 billion tons biomass and further supplies more than 30% of US current petroleum consumption (Sousa, Chundawat, Balan, & Dale, 2009). The total mandates amounts to 21 billion gallons for advanced biofuel by 2022, of which 16 billion gallons must be derived from lignocellulosic feedstock (110th Congress in Washington, 2007). In China, according to Middle and Long Term Development Plan of Renewable Energy formulated by NDRC, the annual bio-ethanol production is targeted at 10 million tons by 2020 (Qiu et al., 2010). Production of ethanol from sugars or starch negatively impacts the economics of the process, thus making ethanol more expensive compared with fossil fuels. Hence, the technology development of producing ethanol has shifted towards the utilization of lignocellulosic materials to lower production costs (Howard, Abotsi, Rensburg, & Howard, 2003).

Pretreatment is considered to be a major unit operation in a biorefinery to convert lignocellulosic biomass into bio-ethanol, which accounts for 16–19% of its total capital (Aden et al., 2002; Wooley, Ruth, Glassner, & Sheehan, 1999). Pretreatment has great potential for efficiency improvement and costs saving through further research and development (Mosier et al., 2005). It is evident that the choice of pretreatment will impact the physicochemical properties of the biomass plant cell wall, it must be introduced prior to the biological steps to overcome this natural recalcitrance and give the high yields vital to economic success (Wyman et al., 2009). These properties will also profoundly affect downstream processes such as enzymatic hydrolysis, fermentation, by-product utilization and residue treatment. Physical, chemical and biological pretreatments are employed nowadays. Among these methods, chemical based pretreatments are considered to be the most promising one for future biorefineries (Sousa et al., 2009). Solvent fractionation pretreatment applies the principle of preferential solubility of various plant cell wall components in different solvents, leading to the disruption of the hydrogen bonding between cellulose segments (Heinze & Koschella, 2005).

In 1952, Walseth (1952) first developed a procedure for producing high reactivity cellulose by swelling air-dried cellulose in 85% H_3PO_4. Whitmore and Atalla (1985) used H_3PO_4 for the regeneration of cellulose I. Cellulose swollen rapidly in 80% phosphoric acid. Warwicker, Bikales, and Segal (1971) reported that cellulose only underwent an interfibrillar swelling at a H_3PO_4 concentration of 80% or less, the dissolution of cellulose occurs at higher H_3PO_4

* Corresponding authors.
E-mail addresses: qinwugx@yahoo.com.cn (W. Qin), cqdong1@163.com (C.-Q. Dong).

0144-8617/$ – see front matter © 2012 Elsevier Ltd. All rights reserved.
http://dx.doi.org/10.1016/j.carbpol.2012.07.068

concentrations (Hudson & Cuculo, 1980). Tracing back to 1995, as a new pharmaceutical excipient, H_3PO_4 had been used to mediate the depolymerization and decrystallization of cellulose, Wei, Kumar, and Banker (1996) found that cellulose with low degrees of crystallinity and polymerization could be prepared.

Zhang, Cui, Lynd, and Kuang (2006) used microcrystalline cellulose to prepare the regenerated amorphous cellulose. 100% cellulose solubilization for regenerated amorphous cellulose was obtained within 3 h. A new lignocellulose pretreatment featuring modest reaction conditions to fractionate lignocellulose into amorphous cellulose, hemicellulose and lignin, by using a series of solvents including concentrated phosphoric acid, acetone and water to separate cell wall components (Zhang et al., 2007), it is possible to decrystallize cellulose fibers, remove part of hemicellulose and lignin. Hemps had been pretreated by Moxley, Zhu, and Zhang (2008) at the optimal condition (84.0% H_3PO_4, at 50 °C, for 60 min). The sugar yield amounted up to 96% after 24 h enzymatic hydrolysis. Kim and Mazza (2008) confirmed the viability of this method. Triticale straw, pine wood were pretreated and hydrolyzed under a known condition, the digestibility reached 98.2% and 74.8%, respectively, suggesting it an effective method for perennial plants and hard woods.

H_3PO_4 is weak triprotic acid, non-toxic and inexpensive comparing to other mineral acids. Phosphoric acid dissolves cellulose more simply, faster and at low temperature. The hydrogen ions from H_3PO_4 could easily diffuse into cellulose (Ramos, Assaf, El Seoud, & Frollini, 2005). Two phenomena occur after dissolution (Zhang et al., 2006), an esterification reaction between hydroxyl groups of cellulose and H_3PO_4 to form cellulose phosphate, and a competition of hydrogen-bond formation among the remaining hydroxyl groups on cellulose chains, a hydrogen ion and a water molecule. Furthermore, cellulose phosphate could be reverted back to free H_3PO_4 and amorphous cellulose through nothing but adding water.

The pretreated cellulose possessed higher accessibility than the un-pretreated one. XRD (X-ray diffraction), AFM (atomic force microscopy) and XPS (X-ray photoelectron spectroscopy) characterization showed that crystalline cellulose partially changed into amorphous cellulose after phosphoric acid pretreatment (Zhang et al., 2006). The amorphous regions bundled with the remaining crystalline structure of cellulose, resulting in the uneven and rough molecular surface. Moreover, the pretreated cellulose could reach the adsorption equilibrium in a relatively shorter time, suggesting that H_3PO_4 pretreatment could accelerate the adsorption rate of enzyme and enhance the subsequent hydrolysis process.

However, the detail physiochemical properties of cellulose in phosphoric acid, acetone and water are still unknown. The cellulose solubility properties in these different solutions have not been systematically explained yet. Herein, cellulose was chosen as our most important research model in lignocellulose structure. Density functional theory (DFT) calculations and molecular dynamic (MD) simulations were applied to cellulose–H_3PO_4 interaction system, cellulose–H_2O interaction system and cellulose–CH_3COCH_3 interaction system, in that DFT calculations and MD simulations are extremely successful approaches to the description of structural and electronic properties for standard bulk materials and complex materials such as biomolecules and interaction system. The physiochemical properties of cellulose in different solutions were firstly detected using DFT. The interactions between cellulose and H_3PO_4, between cellulose and H_2O, between cellulose and CH_3COCH_3 under different temperatures were determined using MD simulations. MD trajectories of cellulose dissolution and precipitation in different solutions were identified and analyzed. Furthermore, the chemical stability of cellulose in different solutions was discussed by calculating the decomposition reactions. This work aims to reveal a fundamental understanding of the dissolution and precipitation phenomenon with temperature effects in the phosphoric acid–acetone pretreatment.

Table 1
Energy bind and HOMO for pure cellulose, H_3PO_4–cellulose system, H_2O–cellulose system, and CH_3COCH_3–cellulose system.

	E_B (eV)	HOMO (eV)
Cellulose		−5.77
Cellulose–phosphoric acid	−1.61	−5.31
Cellulose–water	−0.31	−5.69
Cellulose–acetone	−0.01	−5.65

2. Materials and methods

2.1. Density functional theory calculation

Atomic geometry and electronic structure of H_2O–cellulose, H_3PO_4–cellulose, and CH_3COCH_3–cellulose were computed, respectively, by using DFT with LDA (local-density approximation) to an exchange-correlation functional formulated by Vosko, Wilk, and Nusair (1980), and a double-numeric quality basis set with polarization functions (DNP). LDA is known to be more accurate than generalized gradient approximation (GGA) to describe interlayer coupling in graphite and other van der Waals systems (Janotti, Wei, & Singh, 2001). To improve computational performance, a Fermi smearing of 0.002 hartree (1 hartree = 27.2114 eV) and a global orbital cutoff of 12.5 Å were employed. We focused on interaction between solvent molecule (H_2O, H_3PO_4, and CH_3COCH_3) and cellulose composed of two fragments of double glucose rings with hydrogen bonds between each other. In all the calculations, both the solvent molecule and cellulose were allowed to relax. Calculations were done using an energy convergence tolerance of 1×10^{-6} Ha and a gradient convergence of 1×10^{-6} Ha Å^{-1}. Brillouin zone integration was performed at gamma point (Kudin et al., 2008). Binding energy (E_B) was computed by subtracting the energy of solvent molecule and cellulose from energy of the adsorption system, as shown in Eq. (1).

$$E_B = E\ (\text{cellulose} + \text{solvent}) - E\ (\text{solvent}) - E\ (\text{cellulose}) \quad (1)$$

where E(cellulose + solvent) is the energy of the final optimized configuration, E (solvent) is the energy of solvent molecule, and E (cellulose) is the energy of cellulose. With this definition, a negative E_B value corresponds to a stable adsorption on the surface.

2.2. Molecular dynamics simulations

MD simulation procedures are very popular in biomolecule system. To further investigate the dynamic process of cellulose in complex interaction system in solvents, dynamic molecular simulations were performed with a unique insight into the interaction system to explain the dissolution and precipitation of cellulose in three solvents under different temperature. In the MD simulation, energy minimization is performed to avoid steric clashes for each initial structure of the cellulose–solvent system. The combination of steepest descent and conjugate gradient method is used for the minimization under the conditions of constant pressure and temperature (NPT) ensembles (Phillips et al., 2005). A time step of 1 fs is used to integrate Newton's equation of motion. This simulation protocol helps to ensure the stability of the simulation process. Non-bonded cut-off of 12.5 Å is applied to truncate the long-range interaction to speed up the computation. The particle-mesh Ewald method (PME) algorithm with cubic–spline interpolation (1 Å grid width) is applied to calculate electrostatic interactions efficiently (Darden, York, & Pedersen, 1993).

The potential function is a simple, empirically derived mathematical expression that gives the energy of the interaction system as a function of the positions of the atoms, which can be calculated by the following potential energy function (Levitt, Hirshberg, Sharon, & Daggett, 1995) as the follow Eq. (2):

$$U = \sum_{\text{Bonds}} K_b^i (b_i - b_0^i)^2 + \sum_{\text{Bond angles}} K_\theta^i (\theta_i - \theta_0^i)^2 + \sum_{\text{Torsion angles}} K_\varphi^i \{1 - \cos[n^i(\varphi_i - \varphi_0^i)]\} + \sum_{\substack{\text{Nonbonded\_pairs\_}i,j \\ \text{closer\_than\_cutoff}}} \left[A_{sc}\varepsilon^{ij}\left(\frac{r_0^{ij}}{r_{ij}}\right)^{12} - 2\varepsilon^{ij}\left(\frac{r_0^{ij}}{r_{ij}}\right)^{6} - S_{vdw}(r_{ij}) \right] + 332 \sum_{\substack{\text{Partial\_charges} \\ \text{closer\_thann\_cutoff}}} \left[\frac{q^i q^j}{r_{ij}} - S_{els}^A(r_{ij}) \right] \quad (2)$$

The first three terms in the potential energy function describe the bonded interactions acting between atoms separated by one, two or three covalent bonds, respectively. b_i is the ith bond length with the equilibrium value is b_0^i, K_b^i is the bond stretching force-constant, depending on the type of the ith bond. The second term describes bond angle bending and takes the same form as bond length stretching. The third term describes dihedral (or torsion) angle twisting and is represented by one or more cosine functions, to give a rotation barrier height $2K_\varphi^i$, with a periodicity n^i and an equilibrium value at φ_0^i. The van der Waals interactions are represented by the Lennard-Jones 6–12 potential, which has a term, $\varepsilon^{ij}(r_0{}^{ij}/r^{ij})^{12}$, to account for increasing repulsion as the electron clouds of atoms overlap, and a term, $-2\varepsilon^{ij}(r_0{}^{ij}/r^{ij})^6$, to account for the weak dispersion attraction that exists between all atoms, where r_{ij} is the separation of the atoms. A_{sc} is a scale factor used to reduce the van der Waals repulsion to compensate for the reduced attraction caused by truncation. r_c is the value depending on the cutoff, $q^i q^j/r_{ij}$ is represented by the Coulomb potential, q^i is assigned to all atoms. $S_{vdw}^A(r_{ij})$ and $S_{els}^A(r_{ij})$ are modified by the shifting functions, that compensate for truncation of the interaction at r_c (a cutoff distance).

3. Results and discussion

3.1. Interaction between solvent molecule and cellulose

We theoretically analyze that cellulose interacts to three different solvent molecules including H_2O, H_3PO_4, and CH_3COCH_3, respectively. The interaction of cellulose with H_2O, H_3PO_4, and CH_3COCH_3 was firstly done by dynamic adsorption of H_2O, H_3PO_4, and CH_3COCH_3 to the cellulose molecule in a freedom equilibrium way. Then DFT calculations were performed to do geometric optimization. The stable adsorption models are shown in Fig. 1 and the related binding energy and HOMO (highest occupied molecular orbital) energy are listed in Table 1. As illustrated in Fig. 1a, H_3PO_4 molecule is adsorbed between the two cellulose segments, forming four hydrogen bonds with the binding energy of −1.61 eV. H_3PO_4 molecule is close to the two-CH_2OH belong to each cellulose segment. For the H_2O–cellulose interaction case (Fig. 1b), H_2O approach 1-OH forming one hydrogen bond with the binding energy of −0.31 eV. Comparing H_3PO_4–cellulose system with H_2O–cellulose system, we find that E_B for H_3PO_4–cellulose is four times more than the E_B for H_2O–cellulose system. For the CH_3COCH_3–cellulose interaction case (Fig. 1c), slight interaction

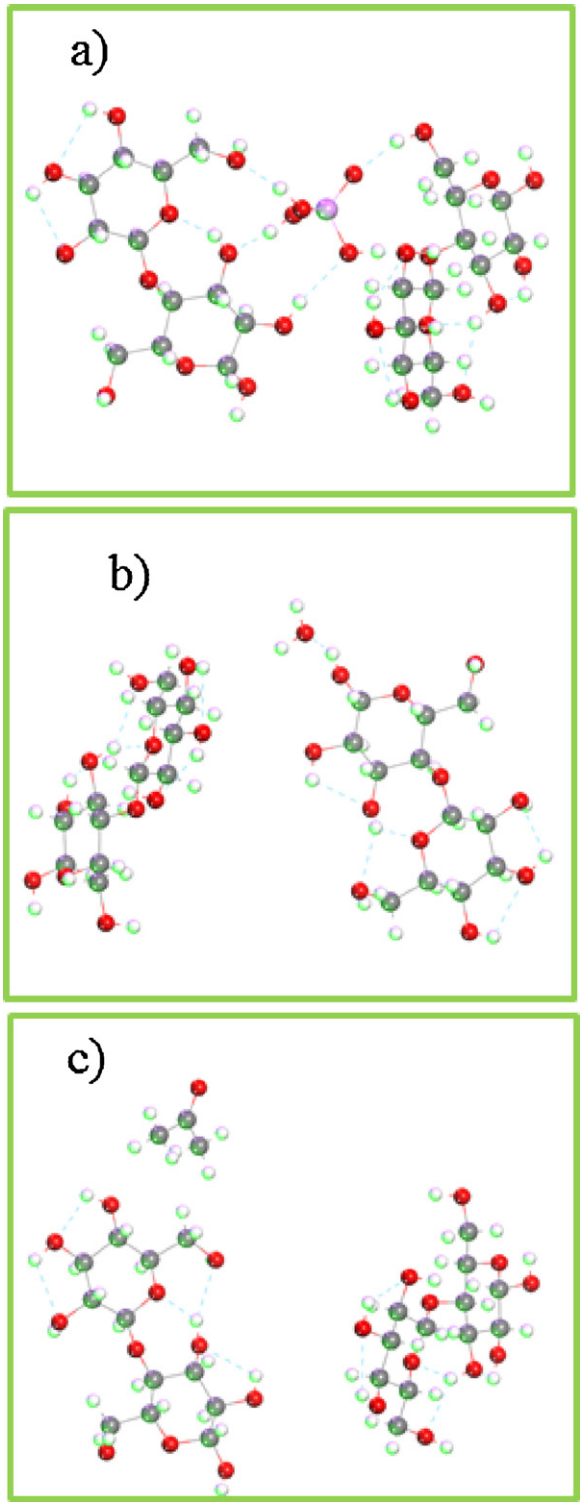

Fig. 1. Stable configuration for (a) H_3PO_4, (b) H_2O, and (c) CH_3COCH_3 interacting to the cellulose segments.

happens between CH_3COCH_3 and cellulose without hydrogen bond, and the binding energy is −0.01 eV, which is far less than E_B for H_2O–cellulose system and H_3PO_4–cellulose system.

Interactions between cellulose and solvent molecules (H_2O, H_3PO_4, and CH_3COCH_3) are further detected by density of state (DOS) analysis, the results of which are depicted in Fig. 2. As shown in Fig. 2, four to five peaks are found below and next to the Fermi energy level (0.00 eV) for pure cellulose and cellulose in

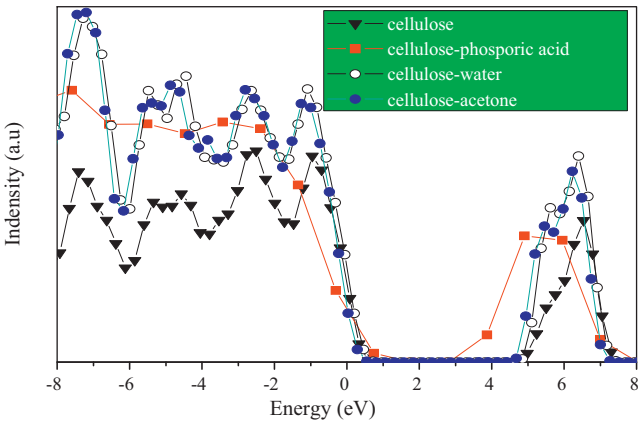

Fig. 2. DOS for pure cellulose, H_3PO_4–cellulose system, H_2O–cellulose system, and CH_3COCH_3–cellulose system.

the H_2O–cellulose system and CH_3COCH_3–cellulose system, while DOS for cellulose in the H_3PO_4–cellulose system delocalizes without obvious peaks. Energy gap for pure cellulose, H_3PO_4–cellulose system, H_2O–cellulose system, and CH_3COCH_3–cellulose system are 5.45 eV, 4.46 eV, 5.38 eV, and 5.48 eV, respectively. Energy gap of H_3PO_4–cellulose system is smaller than E_{gap} of cellulose in other systems. The delocalization of DOS for cellulose in H_3PO_4–cellulose system and the decrease of energy gap suggest that H_3PO_4 could activate cellulose indeed.

3.2. Temperature effect interaction between solvent molecule and cellulose

Temperature is an important factor for the phosphoric acid–acetone pretreatment of lignocellulose, referring to cellulose dissolution and precipitation in different solvents. Therefore, MD simulations in the canonical ensemble are performed under different temperature at atmospheric pressure in the simulation box. The beginning distance between the mass-center of solvent molecule and cellulose molecule is 12.5 Å, at which the potential energy is defined as zero. This separation is large enough while compared to the bond length in both solvent molecule and cellulose molecule, and there is no obvious interaction between two molecules separated by that distance (Kang et al., 2009). Fig. 3 plots the results of MD simulations for cellulose interacting with H_2O, H_3PO_4, and CH_3COCH_3 under three different temperature and constant pressure. The selection of temperature depends on the boiling point of the corresponding solvent molecule. For cellulose–H_3PO_4 interaction system, energy curves refers to 323 K, 343 K and 373 K, show a decrease trend with MD simulation time. Interaction energy decreases quickly at the beginning 100 ps and decreases with a relatively low velocity from 100 to 900 ps, and then reaches about −0.85 eV under 373 K. Potential energy decrease reaches an equilibrium value of about −0.83 eV after 900 ps MD process at 343 K while potential energy shows an equilibrium value of about −0.76 eV after 900 ps MD process at 323 K. It can be observed that potential energy for the cellulose–H_3PO_4 interaction system at the equilibrium state decreases with increase of temperature from 323 to 373 K. However, in the relative high temperature range from 343 to 373 K, potential energy decreases a little with temperature. These results imply that if H_3PO_4 is used for dissolving cellulose and the suitable temperature should be around 343 K.

MD simulation for cellulose–H_2O interaction system at 283 K, 303 K, and 328 K is shown in Fig. 3b that potential energy decreases quickly at before 50 ps during MD simulation, the relative movement and structure adjustment occur with MD process as shown by the fluctuation of the potential energy value with time from 50 to

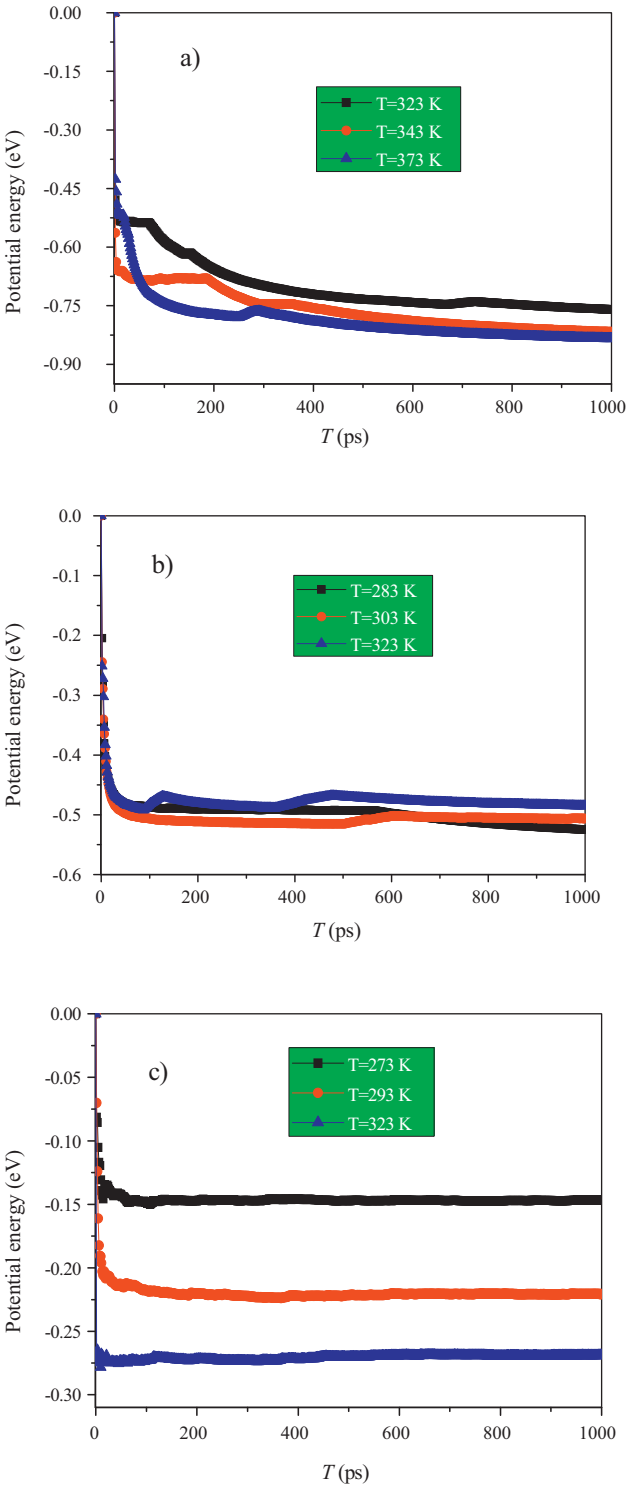

Fig. 3. Potential energy for (a) cellulose–H_3PO_3 interaction system, (b) cellulose–H_2O interaction system, and (c) cellulose–CH_3COCH_3 interaction system under different temperatures.

1000 ps. The equilibrium value at 298 K, 303 K, and 323 K are about −0.47 eV, −0.51 eV, and −0.54 eV, respectively. While compared to the cellulose–H_3PO_4 interaction system, interaction between cellulose and H_2O is more moderate.

For the cellulose–CH_3COCH_3 interaction system, potential energy under the three temperature 273 K, 293K, and 323 K decrease quickly, which imply that MD motion between cellulose and CH_3COCH_3 reaches a balance state in a rapid velocity

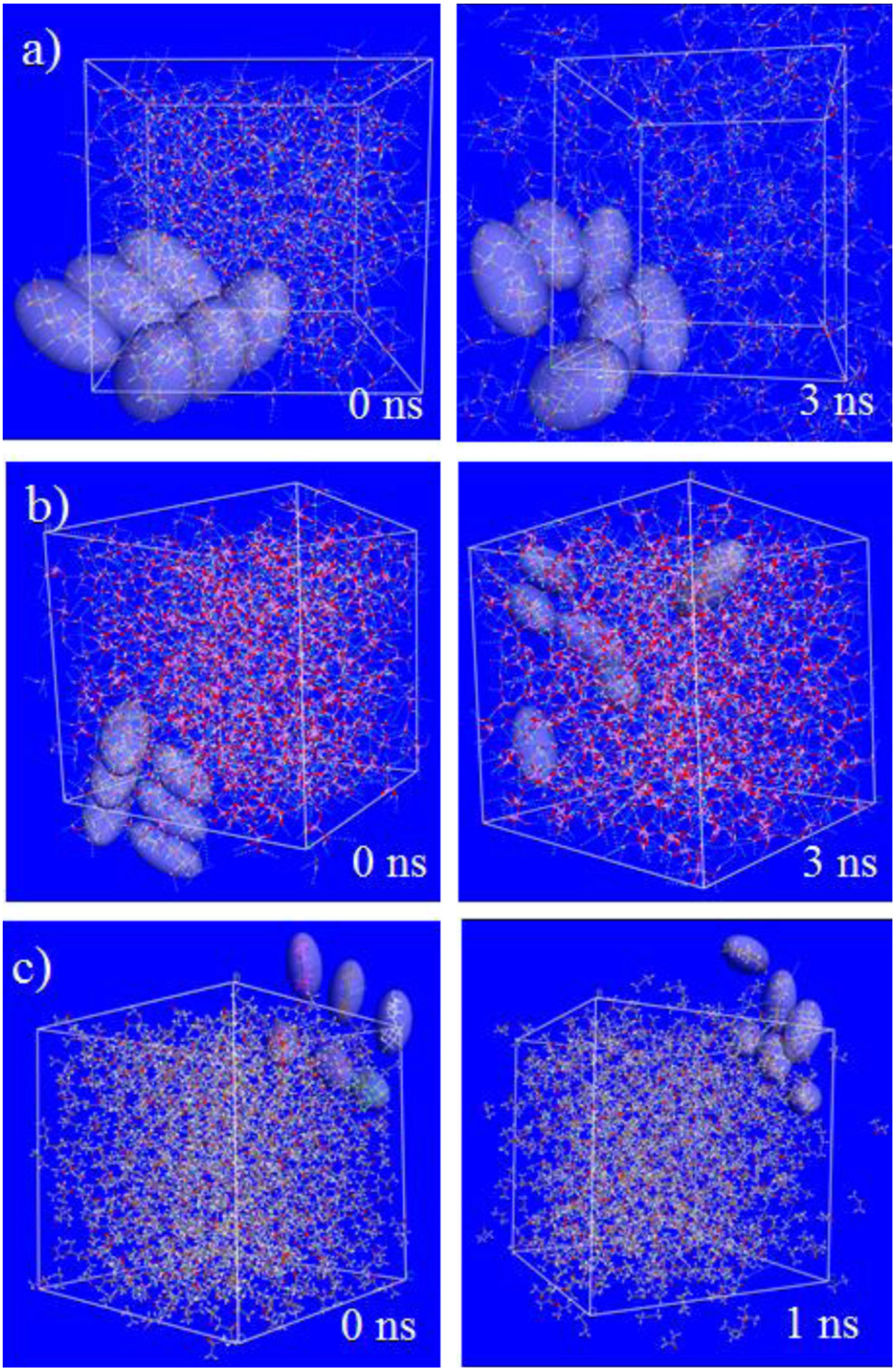

Fig. 4. Snapshots of the process of cellulose dynamic motion in (a) water, (b) phosphoric acid, and (c) acetone.

and the equilibrium potential energy are −0.15 eV, −0.23 eV, and −0.27 eV, respectively. The interaction energy decrease obviously with the decrease of temperature from 323 to 273 K. The temperature effect on the interaction between cellulose and CH_3COCH_3 suggests that low temperature favors the stability of cellulose in CH_3COCH_3.

Comparing cellulose interacting to the three solvent molecules, we found that H_3PO_4 molecule interacts more furious to the cellulose molecule than the other two solvent molecules (water molecule and acetone molecule). In addition, relative high temperature favors the dissolution of cellulose in H_3PO_4, while obvious low temperature favors the precipitation of cellulose in CH_3COCH_3. Such different phenomenon of the two solutions (H_3PO_4, CH_3COCH_3) under high and low temperature suggests that cellulose dissolves more easily in H_3PO_4 at around 343 K and precipitates in CH_3COCH_3 at about 273 K.

3.3. Spontaneous dynamic motion of cellulose in different solvents

MD simulation for a larger cellulose–solvents system was performed to explain and elucidate the interaction mechanism of cellulose in different solvents. Aqueous solution with 800 water molecules and one cellulose segment (made up of six fragments of double glucose rings) was define in the box (29.81 Å × 29.81 Å × 29.81 Å), and then 3 ns MD simulation under 333 K was performed, the results of which was shown in Fig. 4a. Concentrated H_3PO_4 with 400 H_3PO_4 molecules, 340 water molecules, and one cellulose segment (made up of six fragments of double glucose rings) was defined in the box (35.32 Å × 35.32 Å × 35.32 Å), and the related 3 ns MD simulation results under 333 K were shown in Fig. 4b. CH_3COCH_3 with 1000 CH_3COCH_3 molecules and six separating fragments of double glucose rings in a 50.23 Å × 50.23 Å × 50.23 Å box was discussed by doing 1 ns MD simulation, since the cellulose–CH_3COCH_3 interaction system reaches equilibrium more quickly than both cellulose–H_2O and cellulose–H_3PO_4 interaction systems. The results of interaction in CH_3COCH_3 solution under 273 K were indicated in Fig. 4c.

After 3 ns MD process, the cellulose–H_2O solution system under 333 K shows a little movement between the six cellulose fragments of double glucose rings, while the cellulose–H_3PO_4 solution system under 333 K shows dissolution of the cellulose segments, where the six fragments of double glucose rings are separated into the H_3PO_4. However in CH_3COCH_3, part of the six separating fragments of double glucose rings moved toward each other forming hydrogen bond under 273 K after 1 ns MD process. This process corresponds to a flocculation of cellulose fragments. For both cellulose–H_3PO_4 solution system and cellulose–H_2O solution system, the enthalpy decreased in this course chiefly owing to van der Waals interaction, while the entropy increases especially in the cellulose–H_3PO_4 solution system, so that $\Delta G = \Delta H - T\Delta S < 0$. Hence external force or energy is unnecessary to dissolve cellulose in H_3PO_4. However, though both the entropy and the enthalpy of the CH_3COCH_3–cellulose system diminish, the absolute value $|\Delta H|$ is much higher than $|\Delta S|$, resulting in $\Delta G = \Delta H - T\Delta S < 0$. Thus, spontaneous precipitation could be observed, as shown in Fig. 4c.

3.4. Chemical stability of cellulose in different solutions

Inner bond breaking between the glucose rings is discussed to understand the chemical stability of cellulose in different solutions. Fig. 5 depicts the calculated potential energy profiles for the decomposition reaction of cellulose segments in phosphoric acid, acetone, and aqueous solution. Energy barrier (E_a) for cellulose decomposition in acetone, phosphoric acid, and aqueous solution is around 3.301 eV, 3.201 eV, and 3.132 eV, respectively, while the reaction energy (E_r) is 3.332 eV, 3.218 eV, and 3.113 eV. All these reactions are endothermal and all the barrier energy are far higher than 0.75 eV (a magnitude regarded as surmountable for reactions occurring at room temperatures), which imply that cellulose is chemically stable in the three solutions under relatively low temperature.

To further understand the chemical stability of cellulose, we discuss charge transport of cellulose in different solutions. Since the HOMO and LUMO, respectively, mediate the hole and electron transfers through biomaterials, the spatial distributions of HOMO and LUMO are of crucial importance for the charge transfer. The HOMO and LUMO distributions and the related density of state (DOS) for the cellulose at the critical points, i.e. initial state, transition state and final state in different solutions are shown in Fig. 6. According to Fig. 6a, at the initial state, atoms in the right ring of cellulose contribute to the HOMO of cellulose in aqueous solution,

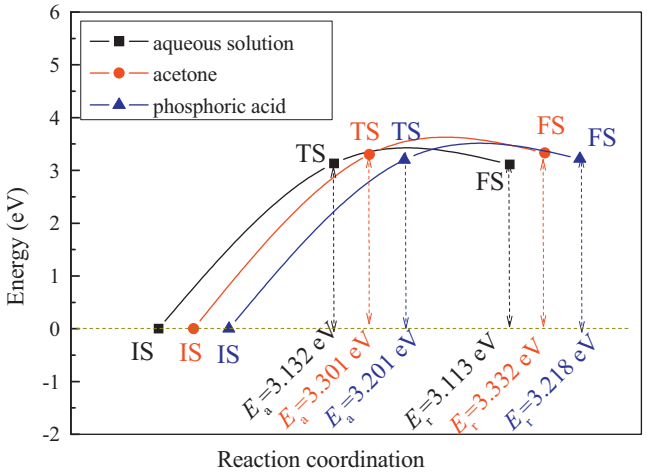

Fig. 5. Potential energy profiles for the decomposition reaction of cellulose segments in phosphoric acid, acetone, and water.

relating to hole transport, while atoms in the left ring of cellulose contribute to the LUMO, relating to the electrons transport. Hence, in the aqueous solution, electrons of atoms in the right ring are excited and then transport to atoms in the left ring. Electron and hole transfer through the main backbone of cellulose. However, when the main backbone of the cellulose decomposed into two rings (the left ring and the right ring) at the transition state and the final state, atoms in the left ring and the glucosidic bond contribute to the HOMO, and atoms in the right ring and the glucosidic bond contribute to the LUMO.

Fig. 6b and c shows that, for the initial state, atoms in the left ring of cellulose contribute to the HOMO of cellulose in acetone and phosphoric acid, while atoms in the left ring of cellulose contribute to the LUMO. The electron transport position in the backbone of cellulose could be regulated using different solutions. In addition, after the main backbone of the cellulose decomposed into two rings (the left ring and the right ring) at the transition state and the final state in acetone and phosphoric acid, atoms in the left ring together with the glucosidic bond of the right ring contribute to the LUMO, and atoms in the right ring together with glucosidic bond between rings contribute to the HOMO, which completely differ from those in aqueous solution. The HOMO and LUMO of the glucosidic bond present its important effect on the charge transport between rings of cellulose.

Analyzing the DOS at the right in Fig. 6a–c, we found that relatively more electron filled below and near to the Fermi level ($E = 0.0$ eV) of rings, especially the left ring of the cellulose before decomposition under aqueous solution, acetone, and phosphoric acid, respectively, than those after decomposition. DOS analysis results suggest that decomposition of cellulose into shorter backbone and the shorter backbone processes higher chemical stability, which corresponds to experiment results. Based on the analysis above, different solution can regulate the electron transport position in the backbone of cellulose, and the glucosidic bond acts as important cross-bridge effect for such charge transport. Decomposition of cellulose into shorter backbone leads to further chemical stability proved by DOS. However, relative long cellulose is also chemically stable enough in aqueous solution, acetone, phosphoric acid, hence, it will be helpful for the non-disruptive pretreatment.

Theoretical calculations above can provide detailed interaction properties of cellulose–H_3PO_4 interaction system, cellulose–H_2O interaction system, and cellulose–CH_3COCH_3 interaction system, it also present the chemical stability of cellulose in different solutions by calculating the decomposition reactions. Although real biomass are much more complicated than the cellulose segment

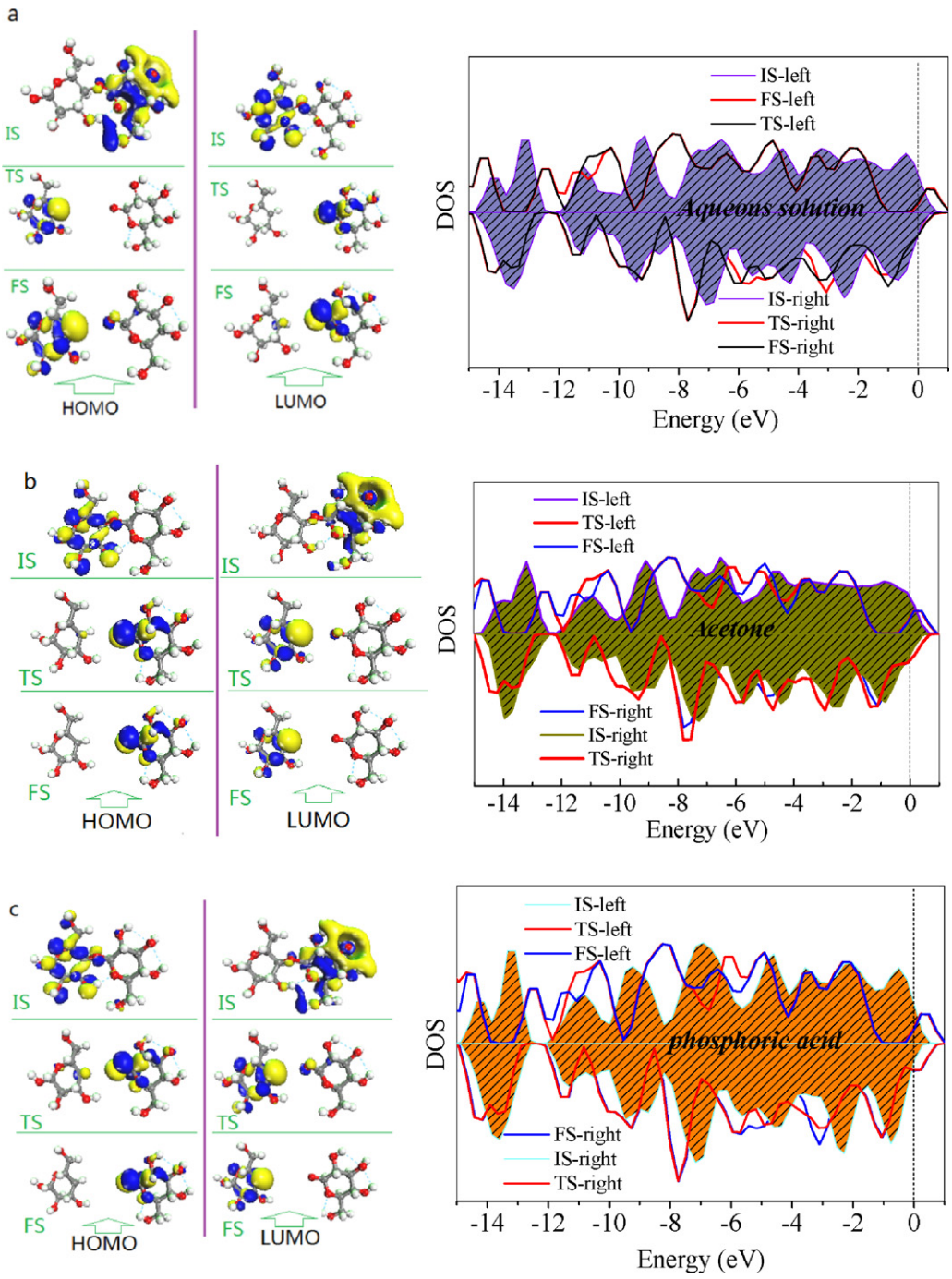

Fig. 6. HOMO, LUMO, and the related DOS for the initial state, transition state, and final state, denoted as IS, TS and FS, respectively, of cellulose in water (a), acetone (b), phosphoric acid (c).

discussed in this work. However, calculation results involved in this paper reveal a fundamental understanding of the solution effect and temperature effect on the cellulose dissolution and precipitation mechanisms.

3.5. Experimental control

We (Kang, Zheng, Qin, Dong, & Yang, 2011) have used phosphoric acid–acetone fractionation to pretreat Chinese white poplar, highly reactive amorphous cellulose could be produced under modest reaction conditions. The feedstock was pretreated at 60 °C with liquid/solid ratio of 8:1 for 1 h, 93.2% cellulose was conserved while more than 40% lignin was removed, majority of the xylan entered into the mixed rinsing liquid in the form of monomeric xylose. Subsequently, over 96.37% enzymatic hydrolysis efficiency (EHE) could be obtained after 24 h enzymatic hydrolysis. Further, our previous experiment results corresponded to the simulations and calculations in this article. During phosphoric acid–acetone pretreatment process, cellulose swollen and dissolved in H_3PO_4 at around 60 °C, when icy CH_3COCH_3 was added in, dissolved cellulose appeared in the form of flocculating solid state, simultaneously, part of lignin dissolved then was separated. Therefore, the

flocculating, amorphous and lignin-removed solid residual is more liable to be hydrolyzed by cellulose. Former experimental results demonstrate the same patterns as our simulations.

4. Conclusion

Mechanism for different solubility properties of cellulose in H_2O, H_3PO_4 and CH_3COCH_3 were simulated and calculated, atomic geometry and electronic properties were computed by using DFT with LDA approximation. H_3PO_4 molecule is adsorbed between the two cellulose segments, forming four hydrogen bonds with E_B of −1.61 eV, which is four times more than E_B for H_2O–cellulose and CH_3COCH_3–cellulose system. DOS for cellulose in the H_3PO_4–cellulose system delocalizes without obvious peak, E_{gap} of 4.46 eV for H_3PO_4–cellulose system is much smaller than E_{gap} in other systems. MD simulation procedures for cellulose–H_3PO_4 interaction system shows the dissolution of the cellulose segments, where the six fragments of double glucose rings are separated into phosphoric acid, then separated fragments moved toward each other forming hydrogen bond and flocculated with the addition of CH_3COCH_3. Also, reaction energy (E_r) in the three solvents are all around 3.5 eV, which are much higher than 0.75 eV, implying that cellulose is chemically stable in these solvents.

Further, our previous experimental results correspond to the simulations and calculations above, cellulose swells and dissolves in H_3PO_4 at 50–70 °C, and the dissolved cellulose flocculates while adding icy CH_3COCH_3, finally the amorphous, flocculating and lignin-removed cellulose becomes more liable to be hydrolyzed to glucoses.

Acknowledgments

The authors thank the financial support for this work provided by National Natural Science Foundation of China (50976032, 51106051), Natural Science Foundation of Beijing (3101001), National Basic Research Program of China (2009CB219801), Fundamental Research Funds for the Central Universities (12MS43, 11QG28), New Century Excellent Talents in University (NCET-10-0374) and National Scientific and Technological Support Plan (2012BAA09B01).

References

In *110th congress* Washington, DC.

Aden, A., Ruth, M., Ibsen, K., Jechura, J., Neeves, K., Sheehan, J., Wallace, B. (2002). Lignocellulosic biomass to ethanol process design and economics utilizing co-current dilute acid prehydrolysis and enzymatic hydrolysis for corn stover. *Technical report*. National Renewable Energy Laboratory (NREL).

British Petroleum Company. (2011). *BP statistical review of world energy*.

Darden, T., York, D., & Pedersen, L. (1993). Particle mesh Ewald: An *N*·log(*N*) method for Ewald sums in large systems. *Journal of Chemical Physics*, *98*(12), 10089–10092.

Heinze, T., & Koschella, A. (2005). Solvents applied in the field of cellulose chemistry: A mini review. *Polimeros*, *15*(2), 84–90.

Howard, R. L., Abotsi, E., Rensburg, E. L., & Howard, S. (2003). Lignocellulose biotechnology: Issues of bioconversion and enzyme production. *African Journal of Biotechnology*, *2*(12), 602–619.

Hudson, S. M., & Cuculo, J. A. (1980). The solubility of unmodified cellulose: A critique of the literature. *Journal of Macromolecular Science Part C: Polymer Reviews*, *18*(1), 6–7.

Janotti, A., Wei, S. H., & Singh, D. J. (2001). First-principles study of the stability of BN and C. *Physical Review B*, *64*(17), 4107–4111.

Kang, Y., Liu, Y. C., Wang, Q., Shen, J. W., Wu, T., & Guan, W. J. (2009). On the spontaneous encapsulation of proteins in carbon nanotubes. *Biomaterials*, *30*(14), 2807–2815.

Kang, P., Zheng, Z. M., Qin, W., Dong, C. Q., & Yang, Y. P. (2011). Efficient fractionation of Chinese white poplar biomass with enhanced enzymatic digestibility and modified acetone–soluble lignin. *Bioresources*, *6*(4), 4705–4720.

Kim, J. W., & Mazza, G. (2008). Optimization of phosphoric acid catalyzed fractionation and enzymatic digestibility of flax shives. *Industrial Crops and Products*, *28*(3), 346–355.

Kudin, K. N., Ozbas, B., Schniepp, H. C., Prudhomme, R. K., Aksay, I. A., & Car, R. (2008). Raman spectra of graphite oxide and functionalized graphene sheets. *Nano Letters*, *8*(1), 36–41.

Levitt, M., Hirshberg, M., Sharon, R., & Daggett, V. (1995). Potential energy function and parameters for simulations of the molecular dynamics of proteins and nucleic acids in solution. *Computer Physics Communications*, *91*(1–3), 215–231.

Mosier, N. S., Wyman, C., Dale, B., Elander, R., Lee, Y. Y., Holtzapple, M., et al. (2005). Features of promising technologies for pretreatment of lignocellulosic biomass. *Bioresource Technology*, *96*(6), 673–686.

Moxley, G., Zhu, Z. G., & Zhang, Y. H. P. (2008). Efficient sugar release by the cellulose solvent-based lignocellulose fractionation technology and enzymatic cellulose hydrolysis. *Journal of Agricultural and Food Chemistry*, *56*(17), 7885–7890.

Phillips, J. C., Braun, R., Wang, W., Gumbart, J., Tajkhorshid, E., Villa, E., et al. (2005). Scalable molecular dynamics with NAMD. *Journal of Computational Chemistry*, *26*(16), 1781–1802.

Qiu, H. G., Huang, J. K., Yang, J., Rozelle, S., Zhang, Y. H., & Zhang, Y. L. (2010). Bioethanol development in China and the potential impacts on its agricultural economy. *Applied Energy*, *87*(1), 76–83.

Ramos, L. A., Assaf, J. M., El Seoud, O. A., & Frollini, E. (2005). Influence of the supramolecular structure and physicochemical properties of cellulose on its dissolution in a lithium chloride/*N*,*N*-dimethylacetamide solvent system. *Biomacromolecules*, *6*(5), 2638–2647.

Sousa, L. D., Chundawat, S. P. S., Balan, V., & Dale, B. E. (2009). 'Cradle-to-grave' assessment of existing lignocellulose pretreatment technologies. *Current Opinion in Biotechnology*, *20*(3), 339–347.

Vosko, S. J., Wilk, L., & Nusair, M. (1980). Accurate spin-dependent electron liquid correlation energies for local spin density calculations: A critical analysis. *Canadian Journal of Physics*, *58*(8), 1200–1211.

Walseth, C. S. (1952). Occurrence of cellulases in enzyme preparations from microorganisms. *Tappi*, *35*, 228–233.

Warwicker, J. O., Bikales, N. M., & Segal, L. (1971). *Cellulose and cellulose derivatives, part IV*. New York: John Wiley & Sons, Inc., pp. 325–379.

Wei, S., Kumar, V., & Banker, G. S. (1996). Phosphoric acid mediated depolymerization and decrystallization of cellulose: Preparation of low crystallinity cellulose—A new pharmaceutical excipient. *International Journal of Pharmaceutics*, *142*(2), 175–181.

Whitmore, R. E., & Atalla, R. H. (1985). Factors influencing the regeneration of cellulose I from phosphoric acid. *International Journal of Biological Macromolecules*, *7*(3), 182–186.

Wooley, R., Ruth, M. F., Glassner, D., & Sheehan, J. (1999). Process design and costing of bioethanol technology: A tool for determining the status and direction of research and development. *Biotechnology Progress*, *15*(5), 794–803.

Wyman, C. E., Dale, B. E., Elander, R. T., Holtzapple, M., Ladisch, M. R., Lee, Y. Y., et al. (2009). Comparative sugar recovery and fermentation data following pretreatment of poplar wood by leading technologies. *Biotechnology Progress*, *25*(2), 333–339.

Zhang, Y. H. P., Cui, J. B., Lynd, L. R., & Kuang, L. R. (2006). A transition from cellulose swelling to cellulose dissolution by *o*-phosphoric acid: Evidence from enzymatic hydrolysis and supramolecular structure. *Biomacromolecules*, *7*(2), 644–648.

Zhang, Y. H. P., Ding, S. Y., Mielenz, J. R., Cui, J. B., Elander, R. T., Laser, M., et al. (2007). Fractionating recalcitrant lignocellulose at modest reaction conditions. *Biotechnology and Bioengineering*, *97*(2), 214–223.